https://doi.org/10.5194/egusphere-2026-3390
Preprint. Discussion started: 3 August 2026

Multi-year Raman-polarization lidar profiling in Central Asia: Seasonal analysis of dust and non-dust optical properties over the ACTRIS site in Dushanbe, Tajikistan

Georg Holger Müller[1,2], Athena Augusta Floutsi[1], Julian Hofer[1], Ronny Engelmann[1], Dietrich Althausen[1], Ulla Wandinger[1], Martin Radenz[1], Moritz Haarig[1], Sabur F. Abdullaev[3], Shohina Khalifaeva[3], Albert Ansmann[1], and Holger Baars[1]

[1]Leibniz Institute for Tropospheric Research (TROPOS), Leipzig, Germany
[2]Leipzig Institute for Meteorology (LIM), University of Leipzig, Leipzig, Germany
[3]S.U. Umarov Physical-Technical Institute of the National Academy of Sciences of Tajikistan, Dushanbe, Tajikistan

Correspondence: Georg Holger Müller (gmueller@tropos.de)

Abstract. Dushanbe, located in Central Asia, resides in the global dust belt, fundamental for the emission and transport of dust. The Central Asian Dust EXperiment (CADEX, 2015 to 2016) provided foundational insights into the optical properties of atmospheric dust in Central Asia by means of lidar observations. A follow-up dataset of high-quality multi-year (2019 to 2025) lidar observations from a newly established Aerosol Clouds and Trace Gases Research Infrastructure (ACTRIS) site in Dushanbe, Tajikistan have been analyzed with the goal to deepen the knowledge of the extent, duration and interannual characteristics of the annual dust cycle in the Central Asian region. The dataset consists of automatically processed lidar data, including the application of the POlarization Lidar and PHOtometer Network (POLIPHON) method to separate the measured total particle backscatter coefficient into a dust and non-dust fraction. The study found a pronounced cycle of the dust backscatter coefficient over the course of several years with low values in winter, also in the planetary boundary layer, and a slow onset of the dust season in spring with an increased occurrence of lofted dust layers. The main dust season spans from July to September with a sharp end in September/October. During summer, non-dust particles, likely local pollution, additionally get lifted above the PBL. The PBL is normally well-mixed and shows rather constant contribution of local pollution. These results show the importance of long-term lidar observations in the Central Asian region and the value of high-quality automated processing of the retrieved data.

1 Introduction

Mineral dust is an integral component of the atmospheric aerosol load, affecting the climate, air quality, ecosystems and human health (Prospero and Lamb, 2003; Baars et al., 2012). Earth's radiation budget is directly affected by mineral dust, since it scatters and absorbs solar and terrestrial radiation (Tegen et al., 1996), but also indirectly, since dust particles act as cloud condensation nuclei (CCN) and ice nucleating particles (INP), thus influencing cloud formation and their properties (Twomey, 1977; Albrecht, 1989). The radiative impact of mineral dust (Sokolik and Golitsyn, 1993; Golitsyn et al., 1993; Nazarov et al., 2010a, b) is dependent on its mineralogical composition, which influences its optical properties and is related to

https://doi.org/10.5194/egusphere-2026-3390
Preprint. Discussion started: 3 August 2026

the source region of the dust particles (Sokolik et al., 1993; Caquineau et al., 2002; Su and Toon, 2011; Schuster et al., 2012; Mamouri et al., 2013). Apart from its radiative impact on climate, mineral dust particles are also negatively affecting human health (Wiggs et al., 2003; Karanasiou et al., 2012; Zhang et al., 2016). In addition, they are influencing the Earth's ecosystem, e.g., acting as fertilizer of large rain forests or, when deposited in the ocean, as driver of phytoplankton production (Zhou et al., 2021; Wang et al., 2023; Nogueira et al., 2021; Madhusoodhanan et al., 2024; Mahowald et al., 2017).

The vertical aerosol distribution is a key factor for the evaluation of the radiative impacts of mineral dust, since these effects are altitude-dependent (Hansen et al., 1997). Lidars are powerful instruments that provide vertically-resolved measurements of the optical and microphysical properties of different aerosol types, including mineral dust (Ansmann and Müller, 2005). To better understand the aforementioned radiative impacts of dust, several lidar-based campaigns have been conducted close to, both, dust source and dust outflow regions. In 2006 and 2008, within the Saharan Mineral Dust Experiment (SAMUM), which comprised of two field campaigns in Morocco and Cabo Verde (Ansmann et al., 2011), the relationship between the shape morphology, size distribution, optical, microphysical and chemical properties of Saharan dust was investigated (Ansmann et al., 2011). In 2013 and 2014 the Saharan Aerosol Long-range Transport and Aerosol-Cloud interaction Experiment (SALTRACE) took place in Barbados also investigated Saharan dust, but with focus on its microphysical and optical characterization after long-range transport, using aircraft in-situ and ground-based remote sensing measurements (Weinzierl et al., 2017; Groß et al., 2015; Haarig et al., 2017b, a). A field campaign, conducted in the city of Dushanbe in Tajikistan, Central Asia, was the Central Asian Dust Experiment (CADEX). From March 2015 to August 2016, CADEX took place in Dushanbe, Tajikistan, with the goal to study the optical and microphysical properties of atmospheric aerosol particles, especially dust, within Central Asia (Hofer et al., 2017, 2020a, b). The BACCHUS (Impact of Biogenic versus Anthropogenic emissions on Clouds and Climate: towards a Holistic Understanding) campaign involved measurements with a PollyXT Raman lidar in Nicosia, Cyprus, in spring 2015, investigating aerosol mixtures as well as characterizing pure aerosol types such as dust from different origins, marine and pollution (Kaduk, 2017). Other field campaigns such as CyCARE (Cyprus Clouds Aerosol and Rain Experiment) (Ansmann et al., 2019a) and A-LIFE (Absorbing aerosol layers in a changing climate - Lifetime and Dynamics) helped to gain crucial knowledge of atmospheric dust (Groß et al., 2025; Teri et al., 2025). Raman lidar measurements of aerosol particles on the Arabian Peninsula were conducted during the Optimization of Aerosol Seeding In rain enhancement Strategies (OASIS) project (Filioglou et al., 2020), characterizing dust and dust mixtures within the atmosphere. The characterization of dust and dust mixtures on Cabo Verde was also recently studied by Gebauer et al. (2026).

The aforementioned campaigns were strongly focused on the Saharan region. The Central Asian region remains still under-sampled, even though it was focused on in CADEX that took place in Dushanbe, Tajikistan. Only a few round-based lidar observations have been already conducted in Central Asia before, namely in Kyrgyzstan (Chen and Sverdlik, 2007; Miller-Schulze et al., 2011; Chen et al., 2013a, b). The interest in observations, especially of dust, in Central Asia is, however, growing, with more recent studies concentrating on measurements in the south of Tajikistan (Bi et al., 2025; Huang et al., 2025).

The CADEX field campaign was a pioneering field campaign in Central Asia, including measurements with an atmospheric lidar of the PollyXT type and a sun-photometer, which is also part of the AErosol RObotic NETwork (AERONET; Holben

https://doi.org/10.5194/egusphere-2026-3390
Preprint. Discussion started: 3 August 2026

et al., 1998, 2001). CADEX lasted from 17 March 2015 until 31 August 2016 (Hofer et al., 2017) and provided the first height-resolved dust optical properties in the region, filling thus a rather critical knowledge gap. Based on 18 months of continuous observations, the optical, microphysical and chemical characteristics of dust were investigated along with the seasonal variability of aerosol layer heights. The CADEX key findings are summarized in Sect. 2.2.1.

CADEX highlighted the importance of height-resolved lidar measurements in the region and in June 2019 an updated PollyXT lidar system has been deployed in Dushanbe permanently as part of PollyNET (Baars et al., 2016; Engelmann et al., 2016). PollyNET is part of the European Aerosol Research Lidar Network (EARLINET; Pappalardo et al., 2014), which is part of the Aerosol, Clouds and Trace Gases Research Infrastructure (ACTRIS; Laj et al., 2024), which is a European research infrastructure dedicated to investigate the atmospheric role and impact of atmospheric constituents such as aerosols, trace gases and clouds. A detailed description of the lidar instrument is provided in Sect. 2.2.2. Data from the extended data set acquired by the continuous lidar measurements in Dushanbe have supported the validation efforts for ATLID (Atmospheric Lidar), a 355 nm high-spectral-resolution lidar (HSRL) onboard the Earth Cloud, Aerosol and Radiation Explorer (EarthCARE; Wehr et al., 2023).

This study provides for the first time insights into the annual cycle and interannual development of the dust and non-dust fraction of particles over the course of 5 years. In contrast to CADEX, the full available dataset was used without manual selection of data. In particular, the seasonality of the particle backscatter coefficient and its separation in a dust and non-dust fraction has been investigated in the lower and middle troposphere on a monthly and seasonal basis.

With the continuous and ongoing lidar measurements in Dushanbe since 2019, this study wants to evaluate the representativeness of the results from CADEX, strongly extending the analysis period, investigating the intra-annual variability of atmospheric aerosols above Dushanbe. Furthermore, this study provides first characteristics of the evolution of vertical dust mass concentration profiles in the Central Asian region which can be further used for regional and global climate models. The investigations regarding the abundance of dust and non-dust aerosol particles and the fundamental seasonal characteristics of atmospheric aerosol particles above Dushanbe can also further synergize with studies investigating for example aerosol cloud interactions within the Central Asian region (Jimenez et al., 2026).

The paper is structured as follows. In Sect. 2, the study region (Sect. 2.1), the previous and ongoing lidar observations in Dushanbe (Sect. 2.2), and the applied methods (Sect. 2.3) are introduced. The results are presented and discussed in Sect. 3 followed by a conclusion and outlook in Sect. 4.

2 Study region, previous activities, and instrumentation

2.1 Study region

Dushanbe, Tajikistan (38°34′ N, 68°46′ E), is located within the global dust belt, which extends from the west coast of North Africa to China, as indicated in Fig. 1. Dry, continental climate prevails in the city. Dushanbe lies in a valley surrounded by mountains (specially in the north, east and west of the city) reaching heights of 4000 m and more. It is in close vicinity to major dust sources such as the Taklamakan, the Karakum and Kyzylkum deserts, but is also influenced by aerosol outflow from the

https://doi.org/10.5194/egusphere-2026-3390
Preprint. Discussion started: 3 August 2026

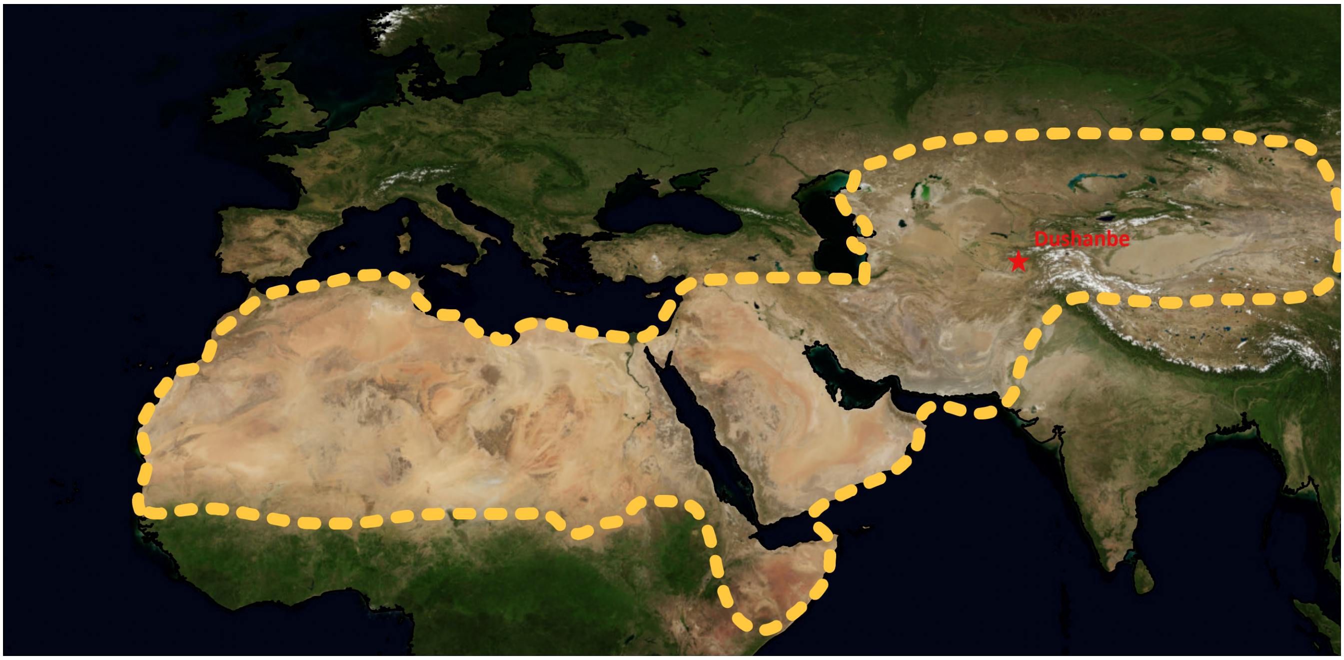

Figure 1. Map of the dust belt (yellow dashed line) region, including the location of Dushanbe, the capital of Tajikistan (indicated with red star); (adapted from: Blue Marble imagery © NASA Earth Observatory, https://science.nasa.gov/earth/earth-observatory/, last access: 10 June 2026).

Aral Sea region, which due to its phenomenal desertification drives an intense dust and salt transport from the exposed sea-bed to the surrounding regions (Banks et al., 2022). The Gobi Desert and deserts areas covering parts of Iran and Afghanistan are also in close proximity to Dushanbe. Due to its location, Dushanbe is frequently exposed to intense dust events (Hofer et al., 2017, 2020a, b).

2.2 Lidar observations in Dushanbe

Lidar and sun-photometer measurements have been conducted, partly accompanied by in-situ measurements of aerosols, at the Poligon measurement site of the Physical Technical Institute of the Academy of Science of Tajikistan (38°33′34″ N, 68°51′22″ E and at an elevation of 864 m height above sea level (a.s.l.); Hofer et al., 2017) since 2015 (Start of CADEX campaign, see below). The site is situated within a rural surrounding of the city of Dushanbe on a slight hill.

2.2.1 CADEX campaign

The Central Asian Dust EXperiment (CADEX) was a joint German-Tajik project that took place in Dushanbe, Tajikistan, from March 2015 to August 2016 (Hofer et al., 2017, 2020a, b) with the main goal to investigate the optical and microphysical properties and the annual cycle of Central Asian mineral dust in the atmosphere. Within this time frame the Poligon measure-

https://doi.org/10.5194/egusphere-2026-3390
Preprint. Discussion started: 3 August 2026

ment site (Hofer et al., 2017) has been equipped with a PollyXT lidar and a sun photometer. The PollyXT lidar (Engelmann et al., 2016) has been operated at three wavelengths (355, 532 and 1064 nm). The extensive dataset acquired over a continuous period of 18 months not only enabled the detailed investigation of single dust outbreaks, but also the temporal evolution of atmospheric aerosols.

The results granted highly valuable insights in the aerosol properties within the atmosphere above Dushanbe. To ensure the usage of high-quality data for the analysis of the CADEX field campaign performed by Hofer et al. (2017, 2020a, b), the vertical profiles retried by the lidar were chosen and analyzed manually. Hofer et al. (2017) found a clear seasonal transition of the aerosol optical depth (AOD) at 500 nm and the Ångstrom exponent with respect to 440 – 870 nm being present between winter and summer in the sun-photometer data acquired during the campaign. While the AOD was highest in the summer season, the fine mode aerosol fraction is behaving the opposite way. This inverse relationship indicates a dust-rich summer season with lowest values of the Ångstrom exponent way below 1 present during summer and higher values above 1 during the winter season. The lidar measurements performed during CADEX (Hofer et al., 2020b) also support these findings with particle linear depolarization ratios retrieved at 355 and 532 nm being highest in summer and lowest in winter. Hofer et al. (2020b) found seasonal mean values of the particle linear depolarization ratio at 355 and 532 nm of 0.14 ± 0.05 and 0.23 ± 0.06 in summer and 0.05 ± 0.02 and 0.09 ± 0.05 in winter, respectively. The lidar-derived Ångström exponent also supports the aforementioned findings.

Additionally, the manual selection of the vertical profiles enabled the creation of an accurate climatology of the predominant geometric aerosol layer height as well as the height of the upmost aerosol layers (Hofer et al., 2020a). The analysis revealed a strong main aerosol layer in late spring and summer up to a height range of 4 to 6.5 km with the upmost layers reaching as high as 11 km. In parallel, the main aerosol layers in winter were situated mainly below 4 km altitude. The selected cases were also analyzed regarding the lidar-derived optical and microphysical properties of the atmospheric aerosol particles. This gave valuable insights into strong dust outbreaks occurring during the summer months, which were able to reach dust mass concentrations of over 2000 $\mu g\, m^{-3}$ in the lower troposphere (Hofer et al., 2017). Nevertheless, local pollution, especially in the planetary boundary layer (PBL) was also occasionally observed as a strong contributor to the total aerosol load.

2.2.2 ACTRIS observational site and instrumentation in Dushanbe, Tajikistan

After the successful lidar deployment in the context of CADEX, a new permanent PollyNET station commenced operations in Dushanbe in June 2019 in the framework of ACTRIS. The PollyNET lidar is also part of EARLINET (European Research Lidar Network, Pappalardo et al., 2014). The station is equipped with a containerized PollyXT lidar system that, compared with the previously deployed PollyXT lidar (Althausen et al., 2009; Hofer et al., 2017), contains additional features (Engelmann et al., 2016, 2019). The lidar operates a diode-pumped laser at 100 Hz. The far-range receiver consists of 8 channels, which enable measurements of the elastically- and Raman-scattered light at the wavelengths of 355, 532, 1064 nm and 387 and 607 nm, respectively, the cross-polarized signal at 355 and 532 nm and the inelastic signal from water vapor at 407 nm. The near-range receiver reduces the height of full overlap of scattered light at 355, 387, 532 and 607 nm to around 60–80 m a.g.l. In addition, the instrument is equipped with a dual-field-of-view depolarization channel at 532 nm (Jimenez et al., 2020b), which

https://doi.org/10.5194/egusphere-2026-3390
Preprint. Discussion started: 3 August 2026

allows the determination of microphysical properties of liquid water droplets (Jimenez et al., 2020a) and enables aerosol-cloud-interaction studies (Jimenez et al., 2026). Data from all 13 channels are acquired with a vertical resolution of 7.5 m and a temporal resolution of 30 s (Engelmann et al., 2016).

In this study, we consider the complete timeseries (i.e., June 2019 to February 2025) from the aforementioned upgraded PollyXT lidar in Dushanbe. Next to the lidar, an AERONET sun-photometer (Cimel CE318) is also operated at the site since the CADEX field campaign.

2.2.3 Airmass source attribution method

Complementing the lidar measurements, airmass source attribution has been performed for a timeframe of five years from 2020 until 2025. For this purpose, the automated time–height-resolved airmass source attribution method TRACE (Radenz, 2021; Radenz et al., 2021) has been employed. Backward simulations with the LPDM Flexpart are combined with land cover classification schemes (Stohl et al., 2005; Pisso et al., 2019). The land cover classification used is a simplified version of the MODIS classification (Friedl et al., 2002), providing seven different surface classes that can influence the passing air parcels. Underlying meteorological data is taken from the Global Forecast Model (GFS) with a resolution of 1° (NCEP, 2000). Air parcels are simulated for a duration of 10 days back in time with emissions every 3 h and 500 m vertically. Air parcels are considered to be influenced by the surface they pass when they fall below a predefined altitude threshold, often referred to as reception height. For this study, a widely used value of 2 km (Val Martin et al., 2018) is used.

Figure 2 shows the simplified MODIS land cover classification. As the figure indicates, the close surroundings of the measurement site in Dushanbe are characterized mostly by a mixture if barren and grass/cropland. While the regions West of Dushanbe, like Persia, the Arabian Peninsula and the North-African deserts like the Saharan desert, mostly consist of barren-typed surface, the northern and southern proximity are dominated by grass and cropland.

2.3 Methodology

2.3.1 Data coverage

For the evaluation of the annual aerosol and dust cycle in Dushanbe, the lidar observations for summer 2019 until the beginning of spring 2025 have been used. A simplified overview of the available data is shown in Fig. 3. Within one month, typically between 500 and 700 datasets are available, which usually corresponds to 24 hourly vertical lidar profiles each day. Due to the differences between the derivation of atmospheric optical properties from the lidar measurements using the Klett- (Klett, 1981, 1985; Fernald, 1984; Sasano et al., 1985) and Raman-method (Ansmann et al., 1990, 1992a, b), results from both retrieval methods are not always available simultaneously. Since the application of the Raman retrieval requires a low background signal to detect inelastic molecular scattering, it is more reliable and often only possible during nighttime. Since, therefore, only nighttime measurements are used and cloudy periods are excluded, the actual fraction of usable vertical profiles available mainly ranges between 20 and 50 % (orange dots).

https://doi.org/10.5194/egusphere-2026-3390
Preprint. Discussion started: 3 August 2026

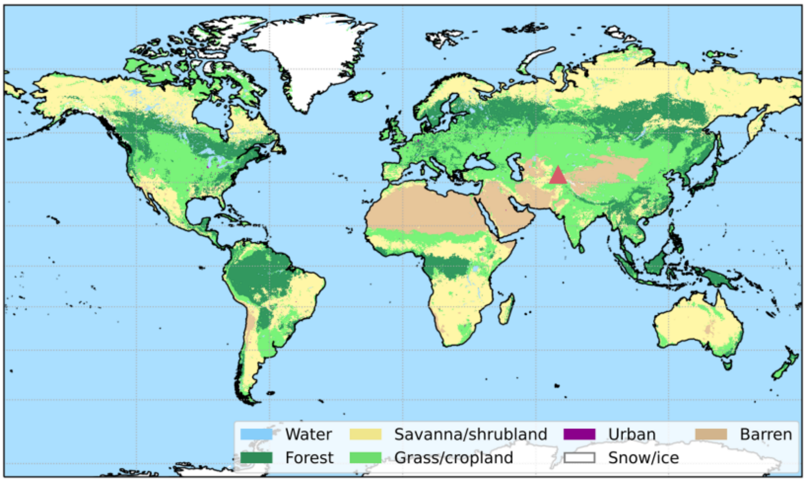

Figure 2. Simplified MODIS land cover classification (adapted from Radenz, 2021). The red triangle represents the location of the measurement site in Dushanbe.

Unfortunately, technical problems with the lidar system caused multiple gaps within the data. The first data gap affected a long period between February 2020 and October 2021. Due to travel restrictions related to the COVID-19 pandemic, a repair of the instrument was not possible. A problem with the laser of the system occurred in the beginning summer 2023 due to short-term power outages scattered over the year. Another issue with the laser forced the shutdown of the system in March 2025. Nevertheless, operation could be resumed in August 2025.

Due to the outages of the system, several analyzed months only show a limited data coverage. For this reason, an additional data selection was performed to increase the representation of the averaged data: months in which less than 100 vertical profiles were available are not included in the following results of monthly averaged data. However, the data is included when analyzing the seasonal characteristics of the measurements, using the data of three continuous months.

2.3.2 Automatic data processing

As introduced above, this study relies on a dataset of fully automatically processed lidar data. The lidar data was processed automatically by the PollyNET processing chain (PPC, Klamt et al., 2024), which is a tool designed to automatically retrieve quality-assured vertical profiles of optical properties in near-real-time (NRT). Retrievals based on both Klett- (Klett, 1981, 1985; Fernald, 1984; Sasano et al., 1985) and Raman-method (Ansmann et al., 1990, 1992a, b) are available as well as further properties such as water vapor and a target classification (Baars et al., 2017). The PPC is constantly improved by adding new features and products. Recently, the first step of the POlarization LIdar PHOtometer Networking method (POLIPHON, Mamouri and Ansmann, 2014, 2017), retrieving dust and non-dust backscatter profiles from the Raman- and Klett-measurements at 355, 532 and 1064 nm, was recently implemented. This step is further being explained in section 2.3.4. Within this study, only the retrievals for 532 nm are used because the POLIPHON separation technique is well established for

https://doi.org/10.5194/egusphere-2026-3390
Preprint. Discussion started: 3 August 2026

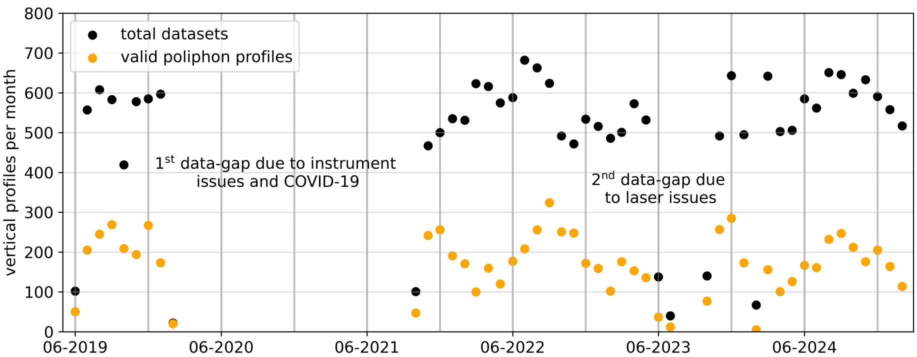

Figure 3. Overview of the number of monthly available profiles, using the aerosol backscatter coefficient derived with the Raman method as reference. Total number of timeframes over which the derivation of a vertical profile was technically suitable for the PPC (black) and the actual count out of this number when profiles were derived for the POLIPHON method (orange).

this wavelength. Quicklooks of the lidar products retrieved by the PPC are available on the PollyNET web-page polly.tropos.de (last access: 10 June 2026). For this study, only the Raman measurements are used. Since the Raman method works best at nighttime, mostly nighttime measurements serve as basis for the analysis.

2.3.3 Post-processing: Cloud screening and data quality

One of the largest sources of errors in the retrieval of aerosol properties from lidar measurements is cloud contamination. Clouds, especially liquid and mixed-phase clouds, are optically thick with respect to the lidar and, therefore, strongly attenuate the signal. They also cause nonphysical artifacts within the lidar signal. High cirrus clouds containing ice may, however, be penetrated by the lidar. Since ice particles are strongly depolarizing, these clouds may be seen as dust-rich aerosol layers and interpreted as such (see Sect. 2.3.4). The PPC already includes a cloud-screening routine to only derive profiles that are not influenced by clouds. In addition, an automated target-classification performed by the PPC based on the retrieved lidar data is used to identify different aerosol and cloud types within the measurement (Baars et al., 2017). Regardless of the cloud screening and the quality assurance routines in place, in some cases cloud-influenced profiles might be still present. Within the PPC, vertical profiles are derived by averaging the signal over a time period, typically in 1 h intervals. This period needs to be flagged as cloud free by the PPC. If clouds are detected via a threshold of the vertical slope within the raw signal, the averaging period is either reduced, thus, avoiding the cloudy period or omitted completely. Nevertheless, random inspections of the data revealed, that some vertical profiles were not correctly screened and showed strong signal peaks caused by clouds within the averaging period. For the profiles which were meant to be used for long-term analysis without further detailed inspection, it is necessary to rely on the automatically processed data to be cloud free.

To ensure the maximum number of cloud-screened profiles possible for the long-term analysis, two additional preliminary steps were considered. In the first approach, the target-classification of the PPC was considered and used to characterize

https://doi.org/10.5194/egusphere-2026-3390
Preprint. Discussion started: 3 August 2026

timeframes of clouds present above the lidar. Although effective and perhaps suitable for future applications, this target-classification based method proved to be not suitable for the present dataset and was therefore not further pursued.

The second approach is the one that has been applied to the data shown within this study, which is a threshold-based method. Different thresholds for the retrieved lidar properties have been found empirically for this study and are applied on the data as such, that the data within the individual vertical profiles exceeding these thresholds is neglected. A threshold of $6\,\mathrm{Mm^{-1}sr^{-1}}$ was found suitable to be applied on the backscatter coefficient at 532 nm. Furthermore, a threshold of 0.60 was applied for the particle linear depolarization ratio at 532 nm. In addition, the lower limit of the reference height of each individual vertical profile was also used as an upper boundary of the profile, which is cut at this respective height.

Although the vertical profiles of the backscatter coefficient and particle linear depolarization ratio reach a full overlap close to the ground, a lower boundary of 700 m a.g.l. has been chosen for the analysis of the vertical profiles. This is mainly due to the profiles of the extinction coefficient being influenced more strongly by the overlap and showing meaningful values above 700 m a.g.l. To enable for later comparisons, this lower boundary is generally applied on all vertical profiles within this study.

2.3.4 POLIPHON method

To quantify the dust and non-dust contributions to the total particle backscatter coefficient measured within the atmosphere, the POLIPHON method has been used. POLIPHON is a powerful approach to link the aerosol optical properties retrieved from lidar measurements to the microphysical properties. In the first step of the POLIPHON method, the measured backscatter signal from the lidar is split into a dust and non-dust fraction using the particle linear depolarization ratio. The separation is performed according to Tesche et al. (2009). Two thresholds for the particle linear depolarization ratio are chosen, above and below which the aerosol particles measured are classified as pure dust or non-dust, respectively. These values are 0.31 as upper threshold, above which pure dust particles are assumed and 0.05 as lower thresholds, below which pure non-dust particles are assumed. The thresholds correspond to the observations at 532 nm. If the measured particle linear depolarization ratio lies in between the two thresholds, an interpolation is performed using the actual measured particle linear depolarization ratio. The first step of the POLIPHON method has already been implemented in the PPC and is automatically applied on the retrieved lidar data within PollyNET. Within this study, the method is only applied on data measured at 532 nm. From the separated backscatter coefficients, the extinction coefficient of the respective aerosol subtype can be calculated using an estimated lidar ratio. For the majority of dust species, Ansmann et al. (2019b) recommend a lidar ratio of 40 sr with the exception of west Saharan dust with a slightly higher lidar ratio of 50 sr. For the conversion within this study, 40 sr have been used. A fixed lidar ratio for dust over the whole timeframe covered by the analysis has been used. However, since the composition of the non-dust aerosol particles may change over the course of time (e.g., between the seasons), choosing one non-dust lidar ratio is more challenging. Therefore, within the scope of this study, only the dust backscatter coefficient has been converted further into an extinction coefficient. The retrieved extinction coefficient can then be used to calculate various microphysical properties, such as the mass, volume and surface concentration as well as the number concentration of different size regimes. This retrieval makes use of correlation studies with AERONET sun photometer measurements (Mamouri and Ansmann, 2014, 2016, 2017). Using these microphysical properties and assuming a supersaturation as well as temperature regime, cloud condensation nuclei (CCN) and

https://doi.org/10.5194/egusphere-2026-3390
Preprint. Discussion started: 3 August 2026

ice nucleating particles (INP) number concentrations can be estimated using empirical parameterizations (Shinozuka et al., 2015; DeMott et al., 2010, 2015) or approaches based on classical nucleation theory (summarized in Ansmann et al., 2021).

Within this study, the dust mass concentration within the atmosphere is derived in addition to the dust and non-dust separation of the particle backscatter coefficient. The dust backscatter coefficient is therefore converted to a dust extinction coefficient using a lidar ratio of 40 sr which is further used to derive the dust mass concentration as described by Mamouri and Ansmann (2016). For the extinction-to-volume conversion factor as well as the density of dust, 0.79 Mm µm^3 cm^{-3} (Ansmann et al., 2019b) and 2.6 g cm^{-3} were used, respectively (Mamouri and Ansmann, 2016). The respective extinction-to-mass conversion with the extinction-to-volume conversion factor was chosen to stay consistent with Hofer et al. (2020a, b) despite the availability of a recently updated set of conversion factors (Ansmann et al., 2026; Hofer et al., 2026). The resulting dust mass concentrations are presented in Sect. 3.4.

2.3.5 Evaluation approach of the dust cycle above Dushanbe

To assess the dust cycle above Dushanbe and its interannual variability, two main steps of averaging the data have been undertaken and are presented in the following. Firstly, all cloud-screened vertical profiles of the backscatter coefficient are averaged to calculate median vertical profiles and 25 to 75 % quartile ranges on a monthly and seasonal basis (e.g., Fig. 4). In a second step, the median vertical profiles are averaged between two selected altitude boundaries. Two height ranges have been chosen for this purpose: 0.7 – 2.0 km and 2.0 – 5.0 km. Within these altitude boundaries, the mean values and standard deviations of the median vertical profiles are calculated (e.g., Fig. 5). By performing these two steps, an analysis of the interannual variability of the atmospheric dust cycle can be performed on a monthly and seasonal basis as well as for multiple altitude ranges.

3 Results and discussion

3.1 Seasonal dust and non-dust vertical backscatter profiles

Both 2022 and 2024 provide continuous data over all seasons. Therefore, the first part of the seasonal analysis of the dust and non-dust backscatter coefficient mainly relies on the data from these years. The seasonal median profiles of the total, dust and non-dust backscatter coefficient of 2022 is given in Fig. 4 panels a – d, for winter, spring, summer and autumn, respectively. The data shows a predominant non-dust fraction for the winter months, with only a small contribution of atmospheric dust. The non-dust fraction can most certainly be attributed to local pollution. Generally, the aerosol load is rather low compared to the rest of the year, with median backscatter coefficient values staying well below 1 Mm^{-1} sr^{-1}. Close to the ground (below 700 m), the backscatter coefficient can be expected to be larger than 1 Mm^{-1} sr^{-1} due to the continental, rather low PBL during winter time, containing a larger amount of aerosol particles than the free troposphere above. Additionally, aerosol particles seem to be confined within the lower part of the troposphere at altitudes below 3 km. This drastically changes within spring, when the total aerosol load of the atmosphere strongly increases. While the non-dust fraction of the particle backscatter coefficient stays roughly the same, compared with the winter season, the dust fraction is significantly increased regarding, both, the magnitude

https://doi.org/10.5194/egusphere-2026-3390
Preprint. Discussion started: 3 August 2026

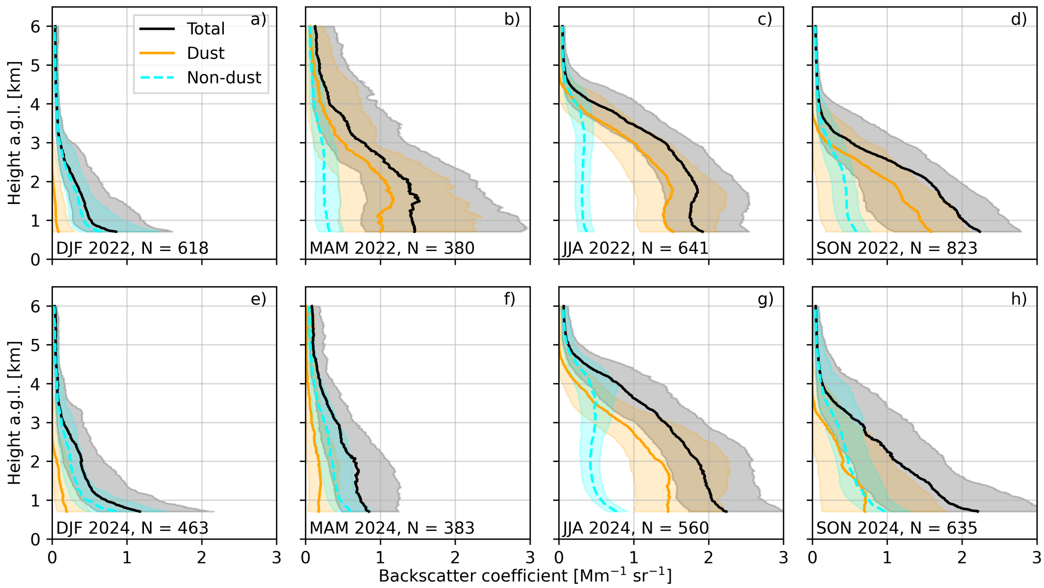

Figure 4. Seasonal median of the vertical profiles of the aerosol backscatter coefficient derived with the Raman method from the lidar measurements in Dushanbe, Tajikistan in 2022 (panels a – d) and 2024 (panels e – h). For each year the winter, spring, summer and autumn season are given along with the number of vertical profiles used per season being indicated with N, respectively. The total backscatter coefficient (black) has been separated in the dust (orange) and non-dust (cyan, dashed) fraction using the POLIPHON method. The shaded areas around the vertical profiles indicate the 25 to 75 % percentile.

and vertical extent, dominating the contribution to the total particle backscatter coefficient. The increased values of the particle backscatter coefficient at altitudes up to 6 km also indicate the presence of lofted aerosol layers. While the non-dust aerosol contribution stays within a similar range throughout the summer season and fall, the dust fraction is again increased in summer compared to spring. However, this increase of the number of dust particles within the lower troposphere comes with a sharp decrease of the aerosol concentration with height and the absence of the signatures of lofted aerosol layers above 5 km within the median profile. Since the 25 to 75 % quartile range of the backscatter coefficient is way narrower in summer compared to spring, a generally higher load of dust aerosol particles with less temporal variability in the atmosphere is identified. In autumn, with the end of the annual dust season, the spread of the 25 to 75 % quartile range gets broader with both conditions of significant aerosol loads compared to summer and low aerosol concentrations being present. The gradual decrease of the altitude in which the median backscatter coefficient becomes nearly 0 Mm^{-1} sr^{-1} from spring to autumn and consequently winter implies the reduced dominance of aerosol and dust layers higher up within the atmosphere over the course of the year, with most aerosol particles in autumn being present in the lowest 4 km of the troposphere.

The described seasonality of 2022 is generally depicting a pronounced annual aerosol cycle within the atmosphere above Dushanbe. However, even when the general seasonality stays the same, substantial interannual variations can be observed when comparing these findings to 2024. The same seasonal climatology of the aerosol backscatter coefficient depicted in Fig. 4 a – d

https://doi.org/10.5194/egusphere-2026-3390
Preprint. Discussion started: 3 August 2026

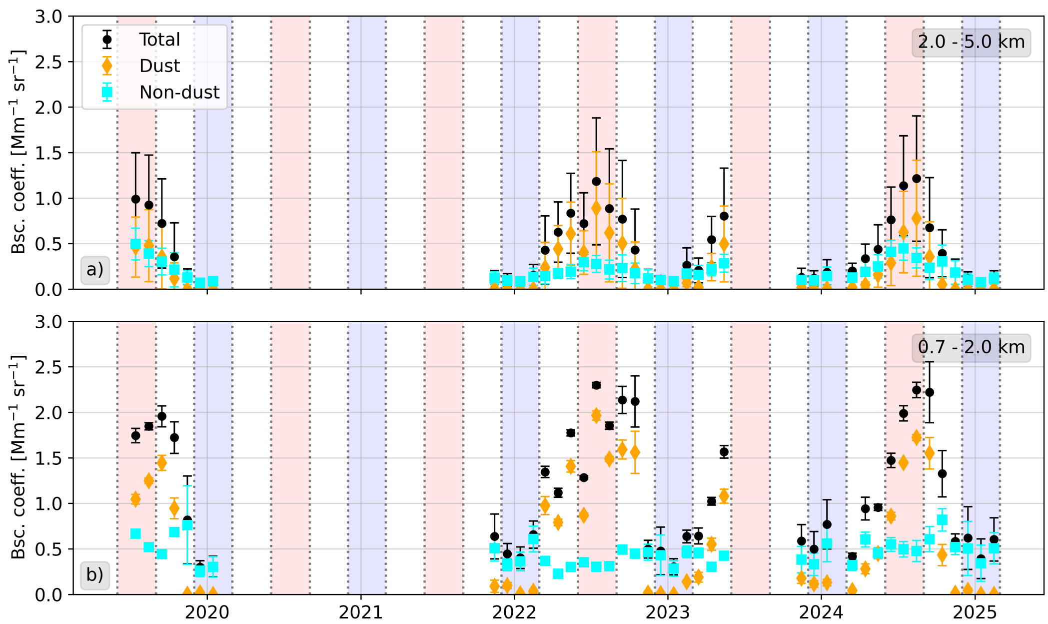

Figure 5. Vertical mean of the monthly median vertical profiles of the particle backscatter coefficient with the standard deviation for the height range between 0.7 and 2.0 km a.g.l. (panel b) and 2.0 and 5.0 km a.g.l. (panel a). The beginning of each year (first January) is indicated by the years given on the horizontal axis; the beginning month of each new season is indicated by the dotted lines. The summer and winter season are additionally highlighted with red and blue shaded areas, respectively.

for 2022 is shown for 2024 in the same figure e – h. While the atmospheric conditions in the winter and summer season are very similar, autumn and especially spring strongly differ between the two years. In spring, the total amount of atmospheric aerosol particles is strongly decreased compared to 2022. Additionally, the measured aerosol backscatter coefficient is dominated by the non-dust fraction, suggesting aerosol types such as pollutants as primary factors of the aerosol particles measured. The dust fraction only contributes in a smaller extent to the measured particle backscatter coefficient, with it being close to the values measured within the winter season. The aerosol load in spring of 2023, which is not shown here due data discontinuities, lies between the measurements of 2022 and 2024, with the dust and non-dust fraction being nearly equal.

As for the non-dust fraction in spring 2024, the non-dust fraction in autumn is also increased compared to 2022 with the seasonal median of the dust and non-dust backscatter coefficient nearly being equal. The aerosol backscatter coefficient is nevertheless close to the measurements of 2022 with an increased non-dust fraction in 2022 compensating a lower dust fraction of the aerosol backscatter coefficient.

3.2 Interannual comparison of the monthly dust and non-dust backscatter coefficient

For a closer investigation of the annual cycle of atmospheric aerosol particles and dust, monthly median vertical profiles of the available single vertical profiles of the backscatter coefficient have been calculated as described in Sect. 2.3.5. For these two

https://doi.org/10.5194/egusphere-2026-3390
Preprint. Discussion started: 3 August 2026

height ranges, the mean of the median backscatter coefficient profile has been calculated and is shown in Fig 5, along with the standard deviation of the vertical median profile of the backscatter coefficient within the height range.

In both height ranges, a clear seasonal cycle of the occurrence of atmospheric aerosol particles can be observed. In the lower layer (see Fig. 5 b), this cycle is mainly driven by the dust fraction. The non-dust fraction is rather constant throughout the year, as discussed above, most likely due to local residential and industrial pollution. A slightly decreased non-dust fraction in 2022 compared with 2019 and 2024/2025 is most likely attributed to interannual variability. This interannual variability is caused mostly by the dust fraction. In winter, a small amount of dust was present within the PBL with the total aerosol load being dominated by the non-dust particle backscatter coefficient. The onset towards the dust season happens in spring with the increase of the dust fraction of the particle backscatter coefficient. Another increase can be seen in summer, where the peak of the dust season happens. In autumn, mainly in September and October, the dust season ends sharply with the dust-related aerosol backscatter coefficient staying high in September, but returning to winter levels until November within about one month. The comparably high standard deviation of the median vertical profile in September and October, observed in all years analyzed, indicates a strongly inclined vertical profile and therefore suggests the gradual decrease of atmospheric dust with altitude. This sharp end of the dust season contrasts the slow buildup taking from March until June/July. Generally, the low standard deviation suggests a low vertical slope of the median backscatter profiles, which is most likely due to turbulent mixing within the PBL and the low troposphere.

In the altitude range of 2.0 to 5.0 km (Fig. 5 a), a similar pattern compared to the altitude range of 0.7 to 2.0 km is observed for the annual dust cycle. Nevertheless, not only the dust fraction of the particle backscatter coefficient shows a clear seasonal cycle, but also the non-dust fraction does, with a peak about a month before the maximum of the respective dust fraction in the same layer. This suggests an increased transport of local pollution in spring and summer into the middle troposphere. Both dust and non-dust cycles, however, show a slower onset and especially decline compared to the PBL and low troposphere and show a higher standard deviation within the median vertical backscatter profiles during the whole year. The peak of the dust season is shorter within the upper layer with the decline in autumn being extended over a longer time, already starting in August/early September.

In both height ranges, strong differences are observed comparing spring 2022 with spring 2024. As already discussed in Sect. 3.1, the non-dust fraction of the aerosol backscatter coefficient is slightly increased throughout spring 2024 compared to 2022, while the dust fraction is strongly reduced. This shows again the interannual variability of the atmospheric aerosol seasonality. In this case, the differences may be at least partly attributed to the differences in the weather patterns throughout the years. Compared to spring 2022, 2024 was colder and lower wind speeds were measured at the airport at Dushanbe. The observed weather also showed more occasions of precipitation, in the beginning of March even in frozen state, in 2024 compared with 2022. The freezing of the ground as well as snow cover may in general be reasons for the low dust fraction of the backscatter coefficient observed in winter and beginning of spring.

Corresponding to the aerosol backscatter coefficient, the mean values of the median monthly vertical profiles of the particle linear depolarization ratio, serving as basis for the POLIPHON method, are shown in Fig. 6. In both height ranges, a similar behavior of the depolarization ratio can be observed with very low values below 0.1 in winter and high values in summer. Since

https://doi.org/10.5194/egusphere-2026-3390
Preprint. Discussion started: 3 August 2026

the values shown represent the measured aerosol mixture present, no statement about the particle linear depolarization of dust can be made. Nevertheless, the observed and averaged particle linear depolarization ratios in summer lie between observations of dust and pollution or dust and smoke and pure dust measurements (Floutsi et al., 2023), partially exceeding 0.25 at 532 nm. The values observed in winter in the lower layers are, however, significantly higher than the values observed typically for pollution and smoke. This indicates either the influence of the low amount of dust present in the PBL or the presence of other depolarizing non-dust particles, e.g., fresh smoke, with a higher particle linear depolarization ratio. In the upper layer, the same pattern can be observed but with slightly reduced mean values of the particle linear depolarization ratio. It should be noted, that for the upper height range and especially in winter, the retrieved particle linear depolarization ratio at 355 nm is slightly higher than at 532 nm. The spectral slope of the measured particle linear depolarization ratio with higher values in the dust season at 532 nm (domination of coarse-mode particles) has been described by Haarig et al. (2017b). Therefore, the measurements of the particle linear depolarization at 355 and 532 nm support the dust and non-dust seasonality.

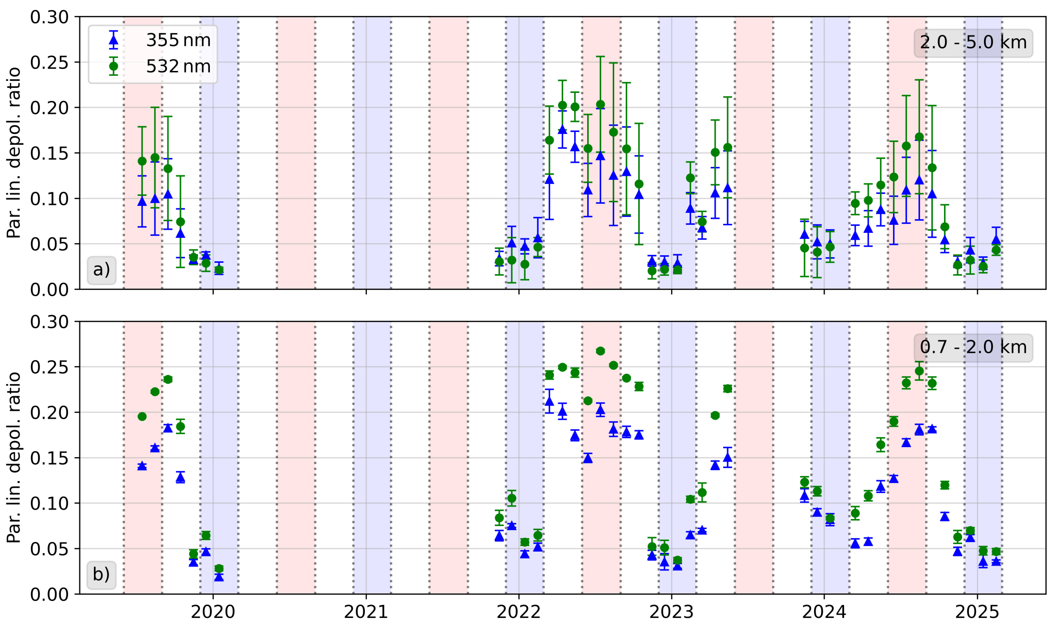

Figure 6. Vertical mean of the monthly median vertical profiles of the particle linear depolarization ratio with the standard deviation at 355 nm (blue triangles) and 532 nm (green circles) for the height range between 0.7 and 2.0 km a.g.l. (panel b) and 2.0 and 5.0 km a.g.l. (panel a). The beginning of each year (January) is indicated by the years given on the horizontal axis; the beginning month of each new season is indicated by the dotted lines. The summer and winter season are additionally highlighted with red and blue shaded areas, respectively.

The seasonal characteristics of the particle linear depolarization ratio visualized in Fig. 6 on a monthly basis can also be generalized on a seasonal basis. Tab. 1 shows the seasonal average of the particle linear depolarization ratio within the upper and lower height ranges, 2.0 – 5.0 and 0.7 – 2.0 km, respectively as well as for 355 and 532 nm. The values given are the means ± the standard deviation of the vertical mean values for the respective height ranges (as they are shown in Fig. 6) for the

https://doi.org/10.5194/egusphere-2026-3390
Preprint. Discussion started: 3 August 2026

Table 1. Average seasonal particle linear depolarization ratio over the whole timeframe of the dataset from July 2019 to February 2025 for two selected height ranges at 355 and 532 nm. The mean values of the monthly vertical profiles of the particle linear depolarization ratio as shown in Fig. 6 have been averaged for all months belonging to the respective season. The resulting mean values ± the standard deviation are given below.

Range [km]	Wavelength [nm]	Par. lin. depol. ratio			
		DJF	MAM	JJA	SON
2.0 – 5.0	355	0.045 ± 0.017	0.106 ± 0.041	0.110 ± 0.021	0.068 ± 0.036
	532	0.039 ± 0.027	0.139 ± 0.047	0.158 ± 0.024	0.076 ± 0.050
0.7 – 2.0	355	0.052 ± 0.022	0.131 ± 0.060	0.164 ± 0.025	0.112 ± 0.060
	532	0.067 ± 0.027	0.181 ± 0.065	0.227 ± 0.027	0.146 ± 0.080

respective months of each season over the whole dataset. As from Fig. 6, the seasonal characteristic of dust in spring, autumn and, especially, summer can be seen. The onset and end of the dust season can again be seen in the comparably high standard deviation in spring and autumn. While the mean values at 532 nm are usually larger than the ones at 355 nm, the measured particle linear depolarization ratio is similar at both wavelengths in winter, with the mean value at 355 nm in the upper height range even exceed the mean at 532 nm, indicating the dominance of non-dust particles.

3.3 Airmass source seasonality

Figure 7 shows the normalized residence time of the air parcels within the reception height, and therefore the influence of the surface, surface types ”barren” or ”grass/cropland”, determined using the TRACE airmass source attribution introduced in Sect. 2.2.3. It is apparent, that the airmasses advected to Dushanbe follow a strong seasonality. In the winter season, the advected airmasses are strongly influenced by their transport across the surface characterized as barren, while airmasses in the summer season are more often originating from regions of grass- and cropland. The change of the dominant airmass source regions might affect the type of aerosol particles advected to Central Asia and also imply an annual change within the aerosol characteristics observed at the measurement site in Dushanbe. Since surfaces classified as barren are mostly found in Northern Africa, the Arabian Peninsula and the close western proximity of Tajikistan, a strong influence of airmasses and therefore aerosols from these regions in winter and spring can be assumed. However, it has to be considered that the dust load within the atmosphere is lower in winter, presumably because of fewer emissions due to snow cover and lower wind speeds. At the end of spring and in summer, the relatively higher influence of grass- and cropland on the normed residence time of the airmasses being advected to Dushanbe is higher compared to the rest of the year. This suggests the advection of these airmasses from local sources around Dushanbe as well as possibly from North-Westerly to North-Easterly regions. Within the summer season and early fall, grass- and cropland can be expected to dry out, making it a possible dust-source too. This confirms the conclusions by Hofer et al. (2020a) made based on their one-year dataset.

https://doi.org/10.5194/egusphere-2026-3390
Preprint. Discussion started: 3 August 2026

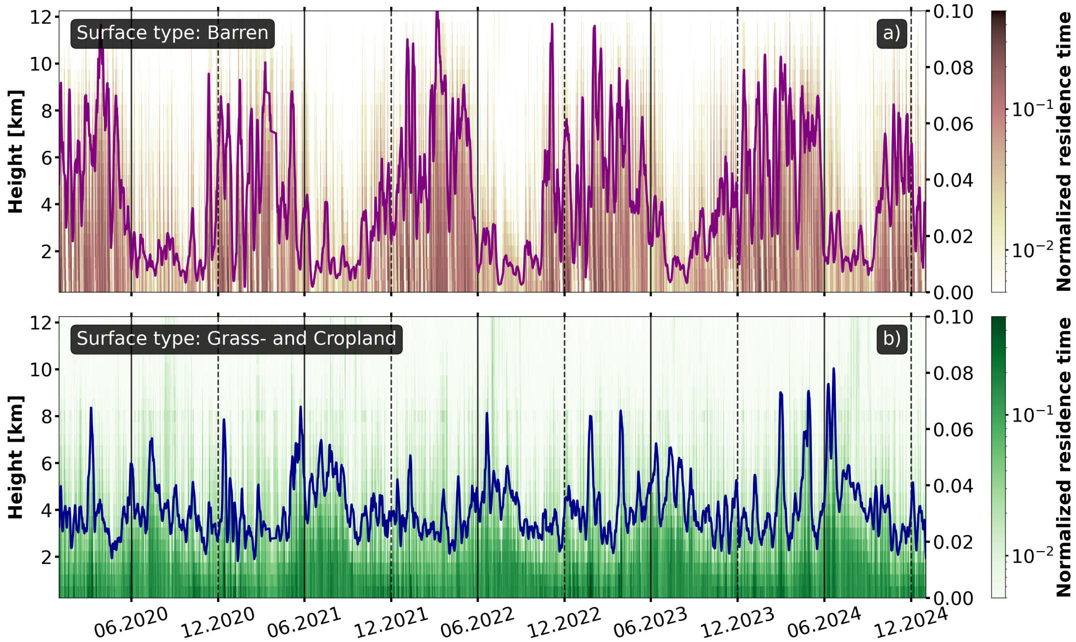

Figure 7. Normalized residence time of airmasses reaching Dushanbe over the surface type ”barren” (panel a) and ”grass- and cropland” (panel b) according to the TRACE backward trajectory model. The reception height has been set to 2 km. The trajectories include the timeframe from the 1 January 2020 to the 1 January 2025 and use the land cover classification given in Fig. 2. The vertical solid and dotted lines indicate the beginning of June and December, respectively, and therefore the summer and winter season. The purple and blue lines (right y-axis) within the panels a and b, respectively, additionally show the mean of the normalized residence time (colorbar at the right side) above barren and grass- and cropland, respectively, from 0 to 12 km at every timestep. A running mean of 7 days has been applied on the averaged normalized residence time.

3.4 Seasonal dust mass concentrations profiles

The vertical profiles of the seasonal median dust mass concentration for the four seasons retrieved using the POLIPHON method are shown in Fig. 8. As the conversion relates the dust backscatter coefficient and the dust mass concentration linearly, the retrieved values show the same characteristics as the results presented in Sect. 3.1. The respective conversions from the dust backscatter coefficient to the dust mass concentration are discussed in Sect. 2.3.4. Generally, the results agree well with the findings from CADEX. Especially the frequent occurrence of high-reaching dust in spring and summer can be seen from Fig. 8. As discussed by Hofer et al. (2017), dust can potentially be deposited within the mountains and on glaciers around Dushanbe, possibly accelerating their melting. The interannual variability in spring and autumn is visible in the median dust mass concentration. It should be noted that the median dust mass concentration profiles of autumn 2023 are likely biased by the absence of measurements in September 2023 and the following slow onset of measurements in October, as indicated in Fig. 3. Nevertheless, the transition function of spring and autumn between the dust-lacking winter season and the dust-rich summer

https://doi.org/10.5194/egusphere-2026-3390
Preprint. Discussion started: 3 August 2026

season (and reversely) can be seen. While the dust mass concentration in 2022 already reached values close to the values at the peak of the dust season during spring, the values of the dust mass concentration during spring in 2024 are closer to the winter level. Although the dust mass concentration stayed at rather low levels during spring 2024, increased values compared to the winter season could be seen in higher altitude, showing patterns comparable with 2023 and 2024. While the median values of the dust mass concentrations are again similar in summer, they, as indicated above, strongly differ in autumn, e.g., with the dust season apparently ending earlier in 2024 and 2019 compared to 2022. The exact reasons for the differences in the extent and duration of the dust season might be interannual differences in advection patterns as well as differences in the meteorological conditions, influencing the emission of dust from local sources, such as wind speeds, precipitation and the extent of frozen grounds. Despite the strong interannual variability observed within the seasonal dust mass concentration, the height for each season in which the dust mass concentration approaches $0\,\mu m/m^3$ is rather constant throughout the years investigated. Therefore it can be assumed that the majority of dust aerosol particles, continuously present within the atmosphere, are confined in a rather constant height range during each season.

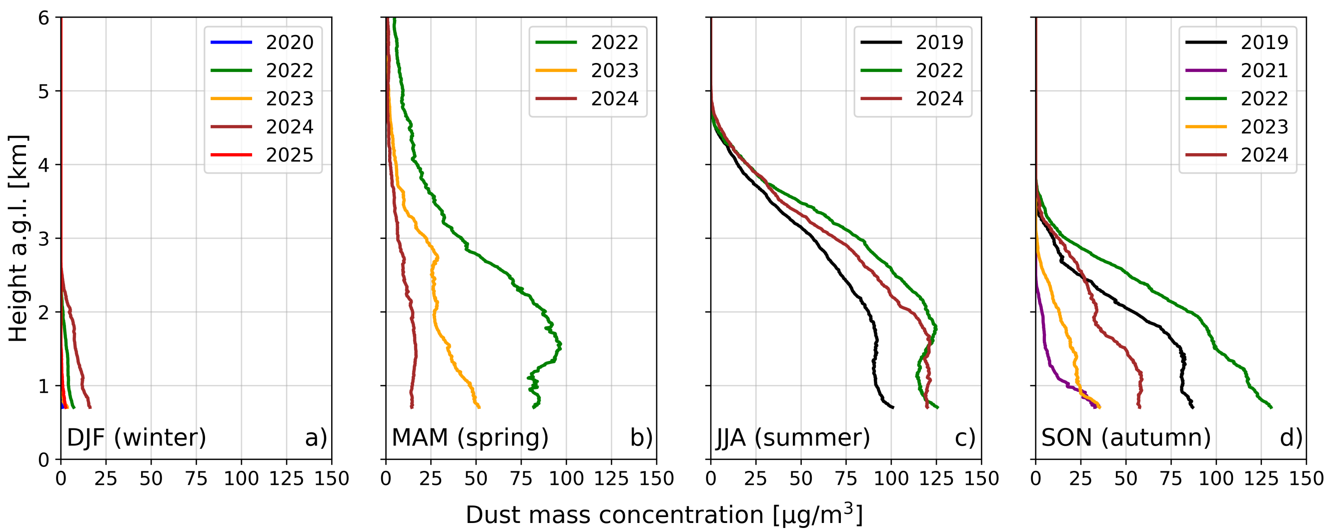

Figure 8. Seasonal median vertical profiles of the dust mass concentration estimated using the POLIPHON method for all investigated years (Summer 2019 – Spring 2025). The estimation was based on the vertical profiles of the aerosol backscatter coefficient retrieved using the Raman method. For the conversion from the backscatter coefficient to an extinction coefficient estimate, a dust lidar ratio of 40 sr was assumed.

4 Conclusion and outlook

Within the presented study, the seasonality of atmospheric dust and non-dust aerosol in Central Asia was evaluated using a novel dataset of long-term, continuous lidar observations in Dushanbe, Tajikistan, from summer 2019 to spring 2025. Analyzing this fully automatically processed set of lidar data, which strongly extends the period of the CADEX field campaign (2015 and 2016), grants valuable insights into the interannual development of the annual dust cycle above Dushanbe.

The dust cycle within the atmosphere has shown a strong interannual variability with respect to its buildup, duration and strength. The main dust season, characterized by dominating dust backscatter coefficient, is clearly identified from July to September, with the dust not only dominating the PBL, but also the troposphere above. The dust season is flanked by a slow buildup of high atmospheric dust concentrations in spring and a rather sharp decrease towards winter, especially evident in September and October. In winter, only low amounts of dust are present even within the lower troposphere. The year-round, vertically-nearly-constant values of the median non-dust backscatter coefficient in the lowermost 0.7 to 2.0 km, indicate the presence of local pollution within the well-mixed PBL. However, the non-dust backscatter coefficient shows a clear seasonality in the atmosphere at altitudes between 2.0 and 5.0 km, indicating lofting of local pollution. Nevertheless, the examination of the seasonal vertical profiles of the backscatter coefficient implies that most aerosol particles present within the atmosphere reside in the lowermost 5.0 km. Seasonal mean values of the particle linear depolarization ratio from 0.7 to 2.0 km of 0.164 ± 0.025 at 355 nm and 0.227 ± 0.027 at 532 nm can be reported for all summer seasons combined. In the winter seasons, these values are comparably smaller with 0.052 ± 0.022 and 0.067 ± 0.027, respectively, and show a less steep spectral slope. Between 2.0 and 5.0 km, the particle linear depolarization at 355 nm is even higher compared to 532 nm. These values as well as the spectral slope identified between 355 and 532 nm show the dominance of dust and non-dust in summer and winter, respectively (Haarig et al., 2017a).

Within the dust season, values of the seasonal median vertical profiles of the dust mass concentrations from 0.7 to 2.0 km determined using the POLIPHON method of up to $125.5\,\mu\mathrm{g/m^3}$ were observed. In winter, the dust mass concentration reaches values of approximately $1.0\,\mu\mathrm{g/m^3}$. Information on the seasonal vertical profiles of the dust mass concentration is important for monitoring air-quality and assessing its climatic impact and may also be valuable for the improvement of atmospheric models.

Overall, the present study not only confirmed the knowledge gained during the time-limited CADEX field campaign in Dushanbe (Hofer et al., 2017, 2020a, b), but also extended it. The frequent occurrence of dust layers in higher altitudes during spring, which was also observed during CADEX, was observed in for the long-term period between 2019-2025. This is important, since dust residing above mountains and glaciers in Central Asia has not been studied yet and needs to be investigated further, as it can potentially impact the snow-covered surfaces either via altering atmospheric radiative effects or directly by settling on top of the snow cover.

The long-term analysis presented here has been enabled by the automatically-derived PPC products and to our knowledge this study is one of the first ones to use the fully automated PPC lidar products. However, the possible cloud contamination, required for an additional data filtering, which has reduced the data coverage in addition to data losses due to technical issues. Both factors do not however affect the findings presented within this study. On the contrary, they motivate the need of continuation of the measurements to further populate the existing dataset, especially in climatic-sensitive regions such as Dushanbe, Tajikistan, which is envisaged in the framework of ACTRIS. It is also planned to further investigate the transport and modification of atmospheric dust in the Central Asian region using ground-based and spaceborne remote sensing.

https://doi.org/10.5194/egusphere-2026-3390
Preprint. Discussion started: 3 August 2026

Code availability. The PPC source code is available at (https://zenodo.org/records/13379737, Klamt et al., 2024). The TRACE source code is available at (https://doi.org/10.5281/zenodo.4438051, Radenz et al., 2021).

Data availability. Currently, the data are available from the authors upon request (gmueller@tropos.de, baars@tropos.de, floutsi@tropos.de).

Author contributions. This study is based on the Bachelor thesis of GHM, supervised by AAF and HB. The paper was conceptualized and written by GHM together with AAF, HB and JH. RE, DA, SFA, SK were responsible for the deployment and operation of the ground-based instruments at Dushanbe. MR performed the TRACE simulations. MH, UW and AA contributed with their expertise on dust optical properties. All co-authors contributed to the scientific discussions and manuscript preparation.

Competing interests. The contact author has declared that none of the co-authors has any competing interests.

Acknowledgements. The CADEX project was funded by the German Federal Ministry of Education and Research (BMBF), now German Federal Ministry of Research, Technology and Space (BMFTR), in the context of "Partnerships for sustainable problem solving in emerging and developing countries" (grant no. 01DK14014). The construction of a new lidar for permanent observations in Tajikistan is funded by the BMBF, now BMFTR, (grant no. 01LK1603A). This project has also received funding from the European Union’s Horizon 2020 research and innovation program ACTRIS-2 Integrating Activities (H2020-INFRAIA-2014-2015, grant no. 654109) and from the European FP7 project by the European Union’s Seventh Framework Program (FP7/2007–2013) collaborative project BACCHUS (grant no. 603445). This activity has received funding from the European Union’s Horizon 2020 research and innovation programme through the ATMO-ACCESS Integrating Activity under grant agreement No 101008004. ACTRIS-D activities are funded by the German Federal Ministry for Education and Research (BMBF, now BMFTR) under the FONA Strategy “Research for Sustainability” (grant no. 01LK2001A).

We gratefully acknowledge the European Space Agency (ESA) for AIRSENSE (Aerosol and aerosol-cloud Interaction from Remote SENSing Enhancement) project through the contract 4000142902/23/I-NS in the framework of the ESA Atmosphere Science Cluster – Research Opportunities 5 – European Coordinated Study on Aerosols and Aerosol/Cloud Interactions.

References

Albrecht, B. A.: Aerosols, Cloud Microphysics, and Fractional Cloudiness, Science, 245, 1227–1230, https://doi.org/10.1126/science.245.4923.1227, 1989.

Althausen, D., Engelmann, R., Baars, H., Heese, B., Ansmann, A., Müller, D., and Komppula, M.: Portable Raman Lidar Polly^{XT} for Automated Profiling of Aerosol Backscatter, Extinction, and Depolarization, J. Atmos. Ocean. Tech., 26, 2366–2378, https://doi.org/10.1175/2009jtecha1304.1, 2009.

Ansmann, A. and Müller, D.: Lidar and Atmospheric Aerosol Particles, In: Weitkamp, C. (eds), Lidar: Range-Resolved Optical Remote Sensing of the Atmosphere, Springer Series in Optical Sciences, 102, pp. 105–141, Springer, New York, https://doi.org/10.1007/0-387-25101-4_4, 2005.

Ansmann, A., Riebesell, M. A., and Weitkamp, C.: Measurement of atmospheric aerosol extinction profiles with a Raman lidar, Opt. Lett., 15, 746–748, https://doi.org/10.1364/OL.15.000746, 1990.

Ansmann, A., Riebesell, M. A., Wandinger, U., Weitkamp, C., Voss, E., Lahmann, W., and Michaelis, W.: Combined raman elastic-backscatter LIDAR for vertical profiling of moisture, aerosol extinction, backscatter, and LIDAR ratio, App. Phys., 55, 18–28, https://doi.org/10.1007/BF00348608, 1992a.

Ansmann, A., Wandinger, U., Riebesell, M. A., Weitkamp, C., and Michaelis, W.: Independent measurement of extinction and backscatter profiles in cirrus clouds by using a combined Raman elastic-backscatter lidar, Appl. Opt., 31, 7113–7131, https://doi.org/10.1364/AO.31.007113, 1992b.

Ansmann, A., Petzold, A., Kandler, K., Tegen, I., Wendisch, M., Müller, D., Weinzierl, B., Müller, T., and Heintzenberg, J.: Saharan Mineral Dust Experiments SAMUM–1 and SAMUM–2: what have we learned?, Tellus B, 63, 403, https://doi.org/10.1111/j.1600-0889.2011.00555.x, 2011.

Ansmann, A., Mamouri, R.-E., Bühl, J., Seifert, P., Engelmann, R., Hofer, J., Nisantzi, A., Atkinson, J. D., Kanji, Z. A., Sierau, B., Vrekoussis, M., and Sciare, J.: Ice-nucleating particle versus ice crystal number concentration in altocumulus and cirrus embedded in Saharan dust: a closure study, Atmos. Chem. Phys., 19, 15 087–15 115, https://doi.org/10.5194/acp-19-15087-2019, 2019a.

Ansmann, A., Mamouri, R.-E., Hofer, J., Baars, H., Althausen, D., and Abdullaev, S. F.: Dust mass, cloud condensation nuclei, and ice-nucleating particle profiling with polarization lidar: updated POLIPHON conversion factors from global AERONET analysis, Atmos. Meas. Tech., 12, 4849–4865, https://doi.org/10.5194/amt-12-4849-2019, 2019b.

Ansmann, A., Ohneiser, K., Mamouri, R.-E., Knopf, D. A., Veselovskii, I., Baars, H., Engelmann, R., Foth, A., Jimenez, C., Seifert, P., and Barja, B.: Tropospheric and stratospheric wildfire smoke profiling with lidar: mass, surface area, CCN, and INP retrieval, Atmos. Chem. Phys., 21, 9779–9807, https://doi.org/10.5194/acp-21-9779-2021, 2021.

Ansmann, A., Hofer, J., Mamouri, R.-E., Haarig, M., Baars, H., and Wandinger, U.: Aerosol optical-to-microphysical conversion factors for lidars and ceilometers from extended AERONET data analyses: POLIPHON update, Atmos. Meas. Tech., 19, 3801–3830, https://doi.org/10.5194/amt-19-3801-2026, 2026.

Baars, H., Ansmann, A., Althausen, D., Engelmann, R., Heese, B., Müller, D., Artaxo, P., Paixao, M., Pauliquevis, T., and Souza, R.: Aerosol profiling with lidar in the Amazon Basin during the wet and dry season, J. Geophys. Res. Atmos., 117, D21 201, https://doi.org/10.1029/2012jd018338, 2012.

Baars, H., Kanitz, T., Engelmann, R., Althausen, D., Heese, B., Komppula, M., Preißler, J., Tesche, M., Ansmann, A., Wandinger, U., Lim, J.-H., Ahn, J. Y., Stachlewska, I. S., Amiridis, V., Marinou, E., Seifert, P., Hofer, J., Skupin, A., Schneider, F., Bohlmann, S., Foth, A.,

https://doi.org/10.5194/egusphere-2026-3390
Preprint. Discussion started: 3 August 2026

Bley, S., Pfüller, A., Giannakaki, E., Lihavainen, H., Viisanen, Y., Hooda, R. K., Pereira, S. N., Bortoli, D., Wagner, F., Mattis, I., Janicka, L., Markowicz, K. M., Achtert, P., Artaxo, P., Pauliquevis, T., Souza, R. A. F., Sharma, V. P., van Zyl, P. G., Beukes, J. P., Sun, J., Rohwer, E. G., Deng, R., Mamouri, R. E., and Zamorano, F.: An overview of the first decade of Polly$^{\mathrm{NET}}$: an emerging network of automated Raman-polarization lidars for continuous aerosol profiling, Atmos. Chem. Phys., 16, 5111–5137, https://doi.org/10.5194/acp-16-5111-2016, 2016.

Baars, H., Seifert, P., Engelmann, R., and Wandinger, U.: Target categorization of aerosol and clouds by continuous multiwavelength-polarization lidar measurements, Atmos. Meas. Tech., 10, 3175–3201, https://doi.org/10.5194/amt-10-3175-2017, 2017.

Banks, J. R., Heinold, B., and Schepanski, K.: Impacts of the Desiccation of the Aral Sea on the Central Asian Dust Life-Cycle, J. Geophys. Res. Atmos., 127, e2022JD036 618, https://doi.org/10.1029/2022JD036618, 2022.

Bi, J., Wang, X., Huang, Z., Abdullaev, S. F., Li, B., Meng, Z., Nozirov, D., and Huang, J.: Diurnal and Nocturnal Dust Aerosol Characteristics at Ayvaj of Southwest Tajikistan Determined From Sun-Sky-Lunar Photometric Measurements, J. Geophys. Res. Atmos., 130, e2024JD042 984, https://doi.org/10.1029/2024jd042984, 2025.

Caquineau, S., Gaudichet, A., Gomes, L., and Legrand, M.: Mineralogy of Saharan dust transported over Northwestern tropical Atlantic Ocean in relation to source regions, J. Geophys. Res. Atmos., 107, AAC 4–1–AAC 4–12, https://doi.org/10.1029/2000JD000247, 2002.

Chen, B. and Sverdlik, L.: Optical and microphysical characteristics of aerosol structures in Central Asia, Int. Conf. on Lasers, Applications, and Technologies 2007: Environmental Monitoring and Ecological Applications; Optical Sensors in Bio, Chemical, and Engineering Technologies; and Femtosecond Laser Pulse Filamentation, 6733, https://doi.org/10.1117/12.753117, 2007.

Chen, B. B., Sverdlik, L. G., Imashev, S. A., Solomon, P. A., Lantz, J., Schauer, J. J., Shafer, M. M., Artamonova, M. S., and Carmichael, G.: Empirical relationship between particulate matter and aerosol optical depth over Northern Tien-Shan, Central Asia, Air Qual. Atmos. Health, 2013, 385–396, https://doi.org/10.1007/s11869-012-0192-5, 2013a.

Chen, B. B., Sverdlik, L. G., Imashev, S. A., Solomon, P. A., Lantz, J., Schauer, J. J., Shafer, M. M., Artamonova, M. S., and Carmichael, G. R.: Lidar Measurements of the Vertical Distribution of Aerosol Optical and Physical Properties over Central Asia, Int. J. Atmos. Sci., 6, 261 546, https://doi.org/10.1155/2013/261546, 2013b.

DeMott, P. J., Prenni, A. J., Liu, X., Kreidenweis, S. M., Petters, M. D., Twohy, C. H., Richardson, M. S., Eidhammer, T., and Rogers, D. C.: Predicting global atmospheric ice nuclei distributions and their impacts on climate, Proc. Natl. Acad. Sci. U.S.A., 107, 11 217–11 222, https://doi.org/10.1073/pnas.0910818107, 2010.

DeMott, P. J., Prenni, A. J., McMeeking, G. R., Sullivan, R. C., Petters, M. D., Tobo, Y., Niemand, M., Möhler, O., Snider, J. R., Wang, Z., and Kreidenweis, S. M.: Integrating laboratory and field data to quantify the immersion freezing ice nucleation activity of mineral dust particles, Atmos. Chem. Phys., 15, 393–409, https://doi.org/10.5194/acp-15-393-2015, 2015.

Engelmann, R., Kanitz, T., Baars, H., Heese, B., Althausen, D., Skupin, A., Wandinger, U., Komppula, M., Stachlewska, I. S., Amiridis, V., Marinou, E., Mattis, I., Linné, H., and Ansmann, A.: The automated multiwavelength Raman polarization and water-vapor lidar Polly$^{\mathrm{XT}}$: the neXT generation, Atmos. Meas. Tech., 9, 1767–1784, https://doi.org/10.5194/amt-9-1767-2016, 2016.

Engelmann, R., Hofer, J., Makhmudov, A. N., Baars, H., Hanbuch, K., Ansmann, A., Abdullaev, S. F., Macke, A., and Althausen, D.: CADEX and beyond: Installation of a new Polly$^{\mathrm{XT}}$ site in Dushanbe, E3S Web Conf., 99, 02 010, https://doi.org/10.1051/e3sconf/20199902010, 2019.

Fernald, F. G.: Analysis of atmospheric lidar observations: some comments, Appl. Opt., 23, 652–653, https://doi.org/10.1364/AO.23.000652, 1984.

Filioglou, M., Giannakaki, E., Backman, J., Kesti, J., Hirsikko, A., Engelmann, R., O'Connor, E., Leskinen, J. T. T., Shang, X., Korhonen, H., Lihavainen, H., Romakkaniemi, S., and Komppula, M.: Optical and geometrical aerosol particle properties over the United Arab Emirates, Atmos. Chem. Phys., 20, 8909–8922, https://doi.org/10.5194/acp-20-8909-2020, 2020.

Floutsi, A. A., Baars, H., Engelmann, R., Althausen, D., Ansmann, A., Bohlmann, S., Heese, B., Hofer, J., Kanitz, T., Haarig, M., Ohneiser, K., Radenz, M., Seifert, P., Skupin, A., Yin, Z., Abdullaev, S. F., Komppula, M., Filioglou, M., Giannakaki, E., Stachlewska, I. S., Janicka, L., Bortoli, D., Marinou, E., Amiridis, V., Gialitaki, A., Mamouri, R.-E., Barja, B., and Wandinger, U.: DeLiAn – a growing collection of depolarization ratio, lidar ratio and Ångström exponent for different aerosol types and mixtures from ground-based lidar observations, Atmos. Meas. Tech., 16, 2353–2379, https://doi.org/10.5194/amt-16-2353-2023, 2023.

Friedl, M. A., McIver, D. K., Hodges, J. C., Zhang, X. Y., Muchoney, D., Strahler, A. H., Woodcock, C. E., Gopal, S., Schneider, A., and Cooper, A.: Global land cover mapping from MODIS: algorithms and early results, Remote Sens. Environ., 83, 287–302, https://doi.org/10.1016/S0034-4257(02)00078-0, 2002.

Gebauer, H., Floutsi, A. A., Hofer, J., Haarig, M., Skupin, A., Engelmann, R., Jimenez, C., Wagner, R., and Baars, H.: Characterization of the annual cycle of atmospheric aerosol over Mindelo, Cabo Verde, by means of continuous multiwavelength lidar observations, Atmos. Chem. Phys., 26, 3439–3465, https://doi.org/10.5194/acp-26-3439-2026, 2026.

Golitsyn, G. S., Shukurov, A. K., Abdullaev, S. F., and Nazarov, B. I.: On the surface air cooling due too dust atmospheric turbidity, In: Golitsyn, G. S., Gillette, D. A., and Johnson, T. (Eds.), Joint Soviet-American Experiment on Arid Aerosol, pp. 67–78, Hydrometeoizdat, St. Petersburg, 1993.

Groß, S., Freudenthaler, V., Schepanski, K., Toledano, C., Schäfler, A., Ansmann, A., and Weinzierl, B.: Optical properties of long-range transported Saharan dust over Barbados as measured by dual-wavelength depolarization Raman lidar measurements, Atmos. Chem. Phys., 15, 11 067–11 080, https://doi.org/10.5194/acp-15-11067-2015, 2015.

Groß, S., Freudenthaler, V., Haarig, M., Ansmann, A., Toledano, C., Mateos, D., Seibert, P., Mamouri, R.-E., Nisantzi, A., Gasteiger, J., Dollner, M., Tipka, A., Schöberl, M., Teri, M., and Weinzierl, B.: Characterization of aerosol over the eastern Mediterranean by polarization-sensitive Raman lidar measurements during A-LIFE – aerosol type classification and type separation, Atmos. Chem. Phys., 25, 3191–3211, https://doi.org/10.5194/acp-25-3191-2025, 2025.

Haarig, M., Ansmann, A., Althausen, D., Klepel, A., Groß, S., Freudenthaler, V., Toledano, C., Mamouri, R.-E., Farrell, D. A., Prescod, D. A., Marinou, E., Burton, S. P., Gasteiger, J., Engelmann, R., and Baars, H.: Triple-wavelength depolarization-ratio profiling of Saharan dust over Barbados during SALTRACE in 2013 and 2014, Atmos. Chem. Phys., 17, 10 767–10 794, https://doi.org/10.5194/acp-17-10767-2017, 2017a.

Haarig, M., Ansmann, A., Gasteiger, J., Kandler, K., Althausen, D., Baars, H., Radenz, M., and Farrell, D. A.: Dry versus wet marine particle optical properties: RH dependence of depolarization ratio, backscatter, and extinction from multiwavelength lidar measurements during SALTRACE, Atmos. Chem. Phys., 17, 14 199–14 217, https://doi.org/10.5194/acp-17-14199-2017, 2017b.

Hansen, J., Sato, M., and Ruedy, R.: Radiative forcing and climate response, J. Geophys. Res. Atmos., 102, 6831–6864, https://doi.org/10.1029/96JD03436, 1997.

Hofer, J., Althausen, D., Abdullaev, S. F., Makhmudov, A. N., Nazarov, B. I., Schettler, G., Engelmann, R., Baars, H., Fomba, K. W., Müller, K., Heinold, B., Kandler, K., and Ansmann, A.: Long-term profiling of mineral dust and pollution aerosol with multiwavelength polarization Raman lidar at the Central Asian site of Dushanbe, Tajikistan: case studies, Atmos. Chem. Phys., 17, 14 559–14 577, https://doi.org/10.5194/acp-17-14559-2017, 2017.

Hofer, J., Ansmann, A., Althausen, D., Engelmann, R., Baars, H., Abdullaev, S. F., and Makhmudov, A. N.: Long-term profiling of aerosol light extinction, particle mass, cloud condensation nuclei, and ice-nucleating particle concentration over Dushanbe, Tajikistan, in Central Asia, Atmos. Chem. Phys., 20, 4695–4711, https://doi.org/10.5194/acp-20-4695-2020, 2020a.

Hofer, J., Ansmann, A., Althausen, D., Engelmann, R., Baars, H., Fomba, K. W., Wandinger, U., Abdullaev, S. F., and Makhmudov, A. N.: Optical properties of Central Asian aerosol relevant for spaceborne lidar applications and aerosol typing at 355 and 532 nm, Atmos. Chem. Phys., 20, 9265–9280, https://doi.org/10.5194/acp-20-9265-2020, 2020b.

Hofer, J., König, L., and Ansmann, A.: Updated POLIPHON conversion factors for lidar and ceilometer applications, https://doi.org/10.5281/zenodo.18346577, Zenodo (dataset), 2026.

Holben, B. N., Eck, T. F., Slutsker, I., Tanré, D., Buis, J. P., Setzer, A., Vermote, E., Reagan, J. A., Kaufman, Y. J., Nakajima, T., Lavenu, F., Jankowiak, I., and Smirnov, A.: AERONET - A Federated Instrument Network and Data Archive for Aerosol Characterization, Remote Sens. Environ., 66, 1–16, https://doi.org/10.1016/S0034-4257(98)00031-5, 1998.

Holben, B. N., Tanré, D., Smirnov, A., Eck, T. F., Slutsker, I., Abuhassan, N., Newcomb, W. W., Schafer, J. S., Chatenet, B., Lavenu, F., Kaufman, Y. J., Castle, J. V., Setzer, A., Markham, B., Clark, D., Frouin, R., Halthore, R., Karneli, A., O'Neill, N. T., Pietras, C., Pinker, R. T., Voss, K., and Zibordi, G.: An emerging ground-based aerosol climatology: Aerosol optical depth from AERONET, J. Geophys. Res. Atmos., 106, 12 067–12 097, https://doi.org/10.1029/2001JD900014, 2001.

Huang, Z., Dong, Q., Zhou, T., Bi, J., Chen, R., Liu, Q., Abdullaev, S. F., Nozirov, D., Alam, K., Wang, T., Li, W., Li, Z., Song, X., and Liu, W.: Vertical distribution, optical properties, and source attribution of summer dust in southern Tajikistan: ground-based observations and model results, Atmos. Environ., 361, 121 514, https://doi.org/10.1016/j.atmosenv.2025.121514, 2025.

Jimenez, C., Ansmann, A., Engelmann, R., Donovan, D., Malinka, A., Schmidt, J., Seifert, P., and Wandinger, U.: The dual-field-of-view polarization lidar technique: a new concept in monitoring aerosol effects in liquid-water clouds – theoretical framework, Atmos. Chem. Phys., 20, 15 247–15 263, https://doi.org/10.5194/acp-20-15247-2020, 2020a.

Jimenez, C., Ansmann, A., Engelmann, R., Donovan, D., Malinka, A., Seifert, P., Wiesen, R., Radenz, M., Yin, Z., Bühl, J., Schmidt, J., Barja, B., and Wandinger, U.: The dual-field-of-view polarization lidar technique: a new concept in monitoring aerosol effects in liquid-water clouds – case studies, Atmos. Chem. Phys., 20, 15 265–15 284, https://doi.org/10.5194/acp-20-15265-2020, 2020b.

Jimenez, C., Hofer, J., Ansmann, A., Lipken, F., Baars, H., Engelmann, R., and und Sabur F. Abdullaev, D. A.: Aerosol-cloud interaction in Central Asia: The role of dust in liquid-water droplet formation processes, in prep., to be submitted to Atmos. Chem. Phys., 2026.

Kaduk, C.: Characterization of the optical properties of complex aerosol mixtures observed with a multiwavelength–Raman–polarization lidar during the 6–weeks BACCHUS campaign in Cyprus in spring 2015, Master thesis, Leipzig Institute for Meteorology, Faculty of Physics and Earth Sciences, Leipzig University, https://www.tropos.de/fileadmin/user_upload/Institut/Abteilungen/Fernerkundung/Daten_PDF/MA_Clara_Kaduk.pdf (last access: 28 July 2026), 2017.

Karanasiou, A., Moreno, N., Moreno, T., Viana, M., de Leeuw, F., and Querol, X.: Health effects from Sahara dust episodes in Europe: Literature review and research gaps, Environ. Int., 47, 107–114, https://doi.org/10.1016/j.envint.2012.06.012, 2012.

Klamt, A., Yin, Z., Floutsi, A. A., Griesche, H., Haarig, M., Radenz, M., Jimenez, C., Gast, B., and Baars, H.: PollyNET: Pollynet Processing Chain version 4.0, Zenodo (software), https://doi.org/10.5281/zenodo.13379737, 2024.

Klett, J. D.: Stable analytical inversion solution for processing lidar returns, Appl. Opt., 20, 211–220, https://doi.org/10.1364/AO.20.000211, 1981.

Klett, J. D.: Lidar inversion with variable backscatter/extinction ratios, Appl. Opt., 24, 1638–1643, https://doi.org/10.1364/AO.25.000833, 1985.

https://doi.org/10.5194/egusphere-2026-3390
Preprint. Discussion started: 3 August 2026

Laj, P., Lund Myhre, C., Riffault, V., Amiridis, V., Fuchs, H., Eleftheriadis, K., Petäjä, T., Salameh, T., Kivekäs, N., Juurola, E., Saponaro, G., Philippin, S., Cornacchia, C., Arboledas, L., Baars, H., Claude, A., De Mazière, M., Dils, B., Dufresne, M., Evangeliou, N., Favez, O., Fiebig, M., Haeffelin, M., Herrmann, H., Höhler, K., Illmann, N., Kreuter, A., Ludewig, E., Marinou, E., Möhler, O., Mona, L., Murberg, L., Nicolae, D., Novelli, A., O'Connor, E., Ohneiser, K., Petracca Altieri, R., Picquet-Varrault, B., van Pinxteren, D., Pospichal, B., Putaud, J., Reimann, S., Siomos, N., Stachlewska, I., Tillmann, R., Voudouri, K., Wandinger, U., Wiedensohler, A., Apituley, A., Comerón, A., Gysel-Beer, M., Mihalopoulos, N., Nikolova, N., Pietruczuk, A., Sauvage, S., Sciare, J., Skov, H., Svendby, T., Swietlicki, E., Tonev, D., Vaughan, G., Zdimal, V., Baltensperger, U., Doussin, J., Kulmala, M., Pappalardo, G., Sundet, S., and Vana, M.: Aerosol, Clouds and Trace Gases Research Infrastructure – ACTRIS, the European research infrastructure supporting atmospheric science, Bull. Am. Meteorol. Soc., 105, E1098–E1136, https://doi.org/10.1175/BAMS-D-23-0064.1, 2024.

Madhusoodhanan, R., Al-Said, T., Sarkar, A., Fernandes, L., Ahmed, A., Yamamoto, T., Thuslim, F., Al-Dousari, A., Al-Zekri, W., Al-Enezi, M., and Al-Ghunaim, A.: Aeolian dust and hydro-biological characteristics: Decoding dust storm impacts on phytoplankton in the northern Arabian Gulf, Sci. Tot. Environ., 911, 168 583, https://doi.org/10.1016/j.scitotenv.2023.168583, 2024.

Mahowald, N. M., Scanza, R., Brahney, J., Goodale, C. L., Hess, P. G., Moore, J. K., and Neff, J.: Aerosol Deposition Impacts on Land and Ocean Carbon Cycles, Curr. Clim. Change Rep., 3, 16–31, https://doi.org/10.1007/s40641-017-0056-z, 2017.

Mamouri, R. E. and Ansmann, A.: Fine and coarse dust separation with polarization lidar, Atmos. Meas. Tech., 7, 3717–3735, https://doi.org/10.5194/amt-7-3717-2014, 2014.

Mamouri, R.-E. and Ansmann, A.: Potential of polarization lidar to provide profiles of CCN- and INP-relevant aerosol parameters, Atmos. Chem. Phys., 16, 5905–5931, https://doi.org/10.5194/acp-16-5905-2016, 2016.

Mamouri, R.-E. and Ansmann, A.: Potential of polarization/Raman lidar to separate fine dust, coarse dust, maritime, and anthropogenic aerosol profiles, Atmos. Meas. Tech., 10, 3403–3427, https://doi.org/10.5194/amt-10-3403-2017, 2017.

Mamouri, R. E., Ansmann, A., Nisantzi, A., Kokkalis, P., Schwarz, A., and Hadjimitsis, D. G.: Low Arabian dust extinction-to-backscatter ratio, Geophys. Res. Lett., 40, 4762–4766, https://doi.org/10.1002/grl.50898, 2013.

Miller-Schulze, J. P., Shafer, M. M., Schauer, J. J., Solomon, P. A., Lantz, J., Artamonova, M., Chen, B., Imashev, S., Sverdlik, L., Carmichael, G. R., and Deminter, J. T.: Characteristics of fine particle carbonaceous aerosol at two remote sites in Central Asia, Atmos. Environ., 45, 6955–6964, https://doi.org/10.1016/j.atmosenv.2011.09.026, 2011.

Nazarov, B. I., Abdullaev, S. F., and Maslov, V. A.: Studies of Temperature Effects of Dust Storms, Izv. Atmos. Ocean. Phys., 46, 475–481, https://doi.org/10.1134/S0001433810040067, 2010a.

Nazarov, B. I., Maslov, V. A., and Abdullaev, S. F.: Optical and Microphysical Parameters of Arid Dust Aerosol, Izv. Atmos. Ocean. Phys., 46, 468–474, https://doi.org/10.1134/S0001433810040055, 2010b.

NCEP: National Centers For Environmental Prediction/National Weather Service/NOAA/U.S. Department Of Commerce: NCEP FNL Operational Model Global Tropospheric Analyses, continuing from July 1999, https://doi.org/10.5065/D6M043C6, 2000.

Nogueira, J., Evangelista, H., de Morisson Valeriano, C., Sifeddine, A., Neto, C., Vaz, G., Moreira, L. S., Cordeiro, R. C., Turcq, B., Aniceto, K. C., Neto, A. B., Martins, G., Barbosa, C. G. G., Godoi, R. H. M., and Shimizu, M. H.: Dust arriving in the Amazon basin over the past 7,500 years came from diverse sources, Commun. Earth Environ., 2, 5, https://doi.org/10.1038/s43247-020-00071-w, 2021.

Pappalardo, G., Amodeo, A., Apituley, A., Comeron, A., Freudenthaler, V., Linné, H., Ansmann, A., Bösenberg, J., D'Amico, G., Mattis, I., Mona, L., Wandinger, U., Amiridis, V., Alados-Arboledas, L., Nicolae, D., and Wiegner, M.: EARLINET: towards an advanced sustainable European aerosol lidar network, Atmos. Meas. Tech., 7, 2389–2409, https://doi.org/10.5194/amt-7-2389-2014, 2014.

https://doi.org/10.5194/egusphere-2026-3390
Preprint. Discussion started: 3 August 2026

Pisso, I., Sollum, E., Grythe, H., Kristiansen, N. I., Cassiani, M., Eckhardt, S., Arnold, D., Morton, D., Thompson, R. L., and Groot Zwaaftink, C. D.: The Lagrangian particle dispersion model FLEXPART version 10.4, Geosci. Model Dev., 12, 4955–4997, https://doi.org/10.5194/gmd-12-4955-2019, 2019.

Prospero, J. M. and Lamb, P. J.: African Droughts and Dust Transport to the Caribbean: Climate Change Implications, Science, 302, 1024–1027, https://doi.org/10.1126/science.1089915, 2003.

Radenz, M.: Software for automated trajectory analysis: TRACE, Zenodo (software), https://doi.org/10.5281/zenodo.2576558, 2021.

Radenz, M., Seifert, P., Baars, H., Floutsi, A. A., Yin, Z., and Bühl, J.: Automated time–height-resolved air mass source attribution for profiling remote sensing applications, Atmos. Chem. Phys., 21, 3015–3033, https://doi.org/10.5194/acp-21-3015-2021, 2021.

Sasano, Y., Browell, E. V., and Ismail, S.: Error caused by using a constant extinction/backscattering ratio in the lidar solution, Appl. Opt., 24, 3929–3932, https://doi.org/10.1364/AO.24.003929, 1985.

Schuster, G. L., Vaughan, M., MacDonnell, D., Su, W., Winker, D., Dubovik, O., Lapyonok, T., and Trepte, C.: Comparison of CALIPSO aerosol optical depth retrievals to AERONET measurements, and a climatology for the lidar ratio of dust, Atmos. Chem. Phys., 12, 7431–7452, https://doi.org/10.5194/acp-12-7431-2012, 2012.

Shinozuka, Y., Clarke, A. D., Nenes, A., Jefferson, A., Wood, R., McNaughton, C. S., Ström, J., Tunved, P., Redemann, J., Thornhill, K. L., Moore, R. H., Lathem, T. L., Lin, J. J., and Yoon, Y. J.: The relationship between cloud condensation nuclei (CCN) concentration and light extinction of dried particles: indications of underlying aerosol processes and implications for satellite-based CCN estimates, Atmos. Chem. Phys., 15, 7585–7604, https://doi.org/10.5194/acp-15-7585-2015, 2015.

Sokolik, I. N. and Golitsyn, G.: Investigation of optical and radiative properties of atmospheric dust aerosols, Atmos. Environ., 27, 2509–2517, https://doi.org/10.1016/0960-1686(93)90021-P, 1993.

Sokolik, I. N., Andronova, A. V., and Johnson, T. C.: Complex refractive index of atmospheric dust aerosols, Atmos. Environ., 27, 2495–2502, https://doi.org/10.1016/0960-1686(93)90021-P, 1993.

Stohl, A., Forster, C., Frank, A., Seibert, P., and Wotawa, G.: Technical note: The Lagrangian particle dispersion model FLEXPART version 6.2, Atmos. Chem. Phys., 5, 2461–2474, https://doi.org/10.5194/acp-5-2461-2005, 2005.

Su, L. and Toon, O. B.: Saharan and Asian dust: similarities and differences determined by CALIPSO, AERONET, and a coupled climate-aerosol microphysical model, Atmos. Chem. Phys., 11, 3263–3280, https://doi.org/10.5194/acp-11-3263-2011, 2011.

Tegen, I., Lacis, A., and Fung, I.: TThe influence on climate forcing of mineral aerosols from disturbed soils, Nature, 380, 419–422, https://doi.org/10.1038/380419a0, 1996.

Teri, M., Gasteiger, J., Heimerl, K., Dollner, M., Schöberl, M., Seibert, P., Tipka, A., Müller, T., Aryasree, S., Kandler, K., and Weinzierl, B.: Pollution affects Arabian and Saharan dust optical properties in the eastern Mediterranean, Atmos. Chem. Phys., 25, 6633–6662, https://doi.org/10.5194/acp-25-6633-2025, 2025.

Tesche, M., Ansmann, A., Müller, D., Althausen, D., Engelmann, R., Freudenthaler, V., and Groß, S.: Vertically resolved separation of dust and smoke over Cape Verde using multiwavelength Raman and polarization lidars during Saharan Mineral Dust Experiment 2008, J. Geophys. Res. Atmos., 114, D13 202, https://doi.org/10.1029/2009JD011862, 2009.

Twomey, S.: The Influence of Pollution on the Shortwave Albedo of Clouds, J. Atmos. Sci., 34, 1149–1152, https://doi.org/10.1175/1520-0469(1977)034<1149:tiopot>2.0.co;2, 1977.

Val Martin, M., Kahn, R. A., and Tosca, M. G.: A Global Analysis of Wildfire Smoke Injection Heights Derived from Space-Based Multi-Angle Imaging, Remote Sens., 10, 1609, https://doi.org/10.3390/rs10101609, 2018.

https://doi.org/10.5194/egusphere-2026-3390
Preprint. Discussion started: 3 August 2026

Wang, X., Wang, Q., Prass, M., Pöhlker, C., Moran-Zuloaga, D., Artaxo, P., Gu, J., Yang, N., Yang, X., Tao, J., Hong, J., Ma, N., Cheng, Y., Su, H., and Andreae, M. O.: The export of African mineral dust across the Atlantic and its impact over the Amazon Basin, Atmos. Chem. Phys., 23, 9993–10 014, https://doi.org/10.5194/acp-23-9993-2023, 2023.

Wehr, T., Kubota, T., Tzeremes, G., Wallace, K., Nakatsuka, H., Ohno, Y., Koopman, R., Rusli, S., Kikuchi, M., Eisinger, M., Tanaka, T., Taga, M., Deghaye, P., Tomita, E., and Bernaerts, D.: The EarthCARE mission – science and system overview, Atmos. Meas. Tech., 16, 3581–3608, https://doi.org/10.5194/amt-16-3581-2023, 2023.

Weinzierl, B., Ansmann, A., Prospero, J. M., Althausen, D., Benker, N., Chouza, F., Dollner, M., Farrell, D., Fomba, W. K., Freudenthaler, V., Gasteiger, J., Groß, S., Haarig, M., Heinold, B., Kandler, K., Kristensen, T. B., Mayol-Bracero, O. L., Müller, T., Reitebuch, O., Sauer, D., Schäfler, A., Schepanski, K., Spanu, A., Tegen, I., Toledano, C., and Walser, A.: The Saharan Aerosol Long-Range Transport and Aerosol–Cloud-Interaction Experiment: Overview and Selected Highlights, Bull. Am. Meteorol. Soc., 98, 1427–1451, https://doi.org/10.1175/BAMS-D-15-00142.1, 2017.

Wiggs, G. F. S., O'hara, S. L., Wegerdt, J., Van Der Meer, J., Small, I., and Hubbard, R.: The dynamics and characteristics of aeolian dust in dryland Central Asia: possible impacts on human exposure and respiratory health in the Aral Sea basin, Geogr. J., 169, 142–157, https://doi.org/10.1111/1475-4959.04976, 2003.

Zhang, X., Zhao, L., Tong, D. Q., Wu, G., Dan, M., and Teng, B.: A Systematic Review of Global Desert Dust and Associated Human Health Effects, Atmosphere, 7, 158, https://doi.org/10.3390/atmos7120158, 2016.

Zhou, H., Yue, X., Lei, Y., Tian, C., Ma, Y., and Cao, Y.: Aerosol radiative and climatic effects on ecosystem productivity and evapotranspiration, Curr. Opin. Environ. Sci. Health, 19, 100 218, https://doi.org/10.1016/j.coesh.2020.10.006, 2021.